Biological effects of chlorogenic acid nanoformulations on colorectal cancer cells

Daniel Tobón-Vélez, Mallorie Tourbin, Ana María Sepúlveda, Ana María Castañeda-Cifuentes, Christine Frances, Johanna Pedroza-Díaz

Journal of Drug Delivery Science and Technology 115 (2026) 107744

Contents lists available at ScienceDirect

Journal of Drug Delivery Science and Technology

journal homepage: www.elsevier.com/locate/jddst

Biological effects of chlorogenic acid nanoformulations on colorectal cancer cells

Daniel Tobón-Vélez [a], Mallorie Tourbin [a,**], Ana María Sepúlveda [b], Ana María Castañeda-Cifuentes [b], Christine Frances [a], Johanna Pedroza-Díaz [b,*]

[a] Laboratoire de Génie Chimique, Université de Toulouse, CNRS, INPT, UT, Toulouse, France
[b] Grupo de Investigación e Innovación Biomédica GI²B, Grupo de Investigación En Biología Médica BioMed, Instituto Tecnológico Metropolitano ITM, Medellín, 050034, Colombia

ARTICLE INFO

Keywords:
Colorectal cancer
Chlorogenic acid
Encapsulation
Nanospray drying
Cell culture

ABSTRACT

The nanoencapsulation of chlorogenic acid (CGA) by nanospray drying was investigated as a protective bioactive delivery strategy. This study aimed to develop CGA-loaded nanoparticles (NPs) for potential application in colorectal cancer (CRC) therapy using the SW480 and HT-29 cell lines. Eight formulations were prepared with biopolymers—maltodextrin (MD), arabic gum (AG), starch (S), carboxymethyl cellulose (CMC), and hydroxypropyl methylcellulose (HPMC)—and the surfactant polysorbate 80 (PS80). The formulations were transformed into fine powders through nanospray drying and comprehensively characterized using physicochemical techniques. *In vitro* cytotoxicity and proliferation assays were performed using the MTT method across CGA concentrations from 0 to 400 μM. In addition, cell cycle analysis was performed by flow cytometry in HT-29 cells treated with formulations F1 (MD:CGA, 2:1) and F3 (AG:CGA, 2:1). Systems based on MD, AG, and S yielded spherical, smooth particles with an average diameter of about 360 nm, whereas those based on CMC and HPMC produced smaller particles of about 251 nm, likely due to lower polymer concentrations. Unloaded NPs exhibited low overall cytotoxicity in both SW480 and HT-29 CRC cell lines, confirming their biocompatibility. In contrast, CGA-loaded formulations induced a greater reduction in cell viability and proliferation, particularly in HT-29 cells. Cell cycle analysis revealed a slight increase in the sub-G1 population, with F1 promoting S-phase accumulation and F3 causing G2/M arrest. Among all formulations, those containing AG demonstrated significantly enhanced anticancer activity in CRC cells compared with free CGA. This effect appears to be cytostatic rather than apoptotic, suggesting a promising direction for further exploration.

1. Introduction

Cancer is one of the non-communicable diseases with the highest mortality rate worldwide [1]. According to the Global Cancer Observatory, colorectal cancer (CRC) is among the most common cancers, ranking third in incidence and fourth in mortality in both sexes [2]. Sporadic CRC accounts for approximately 75–80 % of all cases and is associated with modifiable risk factors such as diet, lifestyle, alcohol consumption, sedentary behavior, obesity, and tobacco use. Non-modifiable risk factors, including age and genetic predisposition, represent 20–25 % of cases [3].

Treatment mainly relies on surgical resection and systemic therapies such as chemotherapy. However, these approaches are less effective in advanced disease stages, due to molecular alterations that promote treatment evasion and tumor resistance. Additionally, tumor site and location influence survival rates and recurrence risk [4,5]. Different strategies have been explored to improve existing therapies, such as the combination of various chemotherapeutic agents, targeted therapies, and immunotherapies. Nonetheless, toxicity and other side effects derived from these treatments remain issues to be addressed [6].

Phenolic compounds are secondary plant metabolites with high biological activity. Their consumption has been shown to improve quality of life, making them of great interest as potential adjuvants in cancer treatment [7]. Chlorogenic acid (CGA), one of the most abundant phenolic compounds in nature and a major component of coffee, is an ester of caffeic and quinic acids. Previous studies have demonstrated its

* Corresponding author.
** Corresponding author.
E-mail addresses: mallorie.tourbin@toulouse-inp.fr (M. Tourbin), ninipedroza@itm.edu.co (J. Pedroza-Díaz).

https://doi.org/10.1016/j.jddst.2025.107744
Received 6 May 2025; Received in revised form 27 October 2025; Accepted 1 November 2025
Available online 7 November 2025

anticancer properties and its ability to modulate signaling pathways involved in CRC progression [8,9].

However, many studies have reported problems related to CGA absorption. Only about one-third of the ingested compound is absorbed intact in the small intestine, while the remainder is hydrolyzed by esterases into caffeic and quinic acids [10]. Epidemiological studies show a significant difference between the amount of CGA absorbed and that excreted in urine. In addition, CGA exhibits poor membrane permeability due to its high polarity and multiple hydroxyl groups, which limit passive diffusion. Its low lipophilicity also restricts transcellular transport across lipid bilayers, which explains the need for high doses in *in vitro* treatments [11,12].

In search of solutions, nanoencapsulation has been considered as a strategy to improve the bioavailability and absorption of natural products. Studies on polyphenols such as curcumin, quercetin, and other molecules have shown enhanced efficiency in cancer treatments through this approach [13–18]. Consequently, the present study aims to investigate the use of different nanoencapsulated CGA formulations and their therapeutic implications in *in vitro* models of CRC.

Several techniques can be used for nanoscale encapsulation, yielding particles between 10 and 1000 nm [19]. Spray drying is an efficient encapsulation technique that, in a single step, transforms solutions, emulsions, and suspensions into solid particles. Nanospray drying enables the production of smaller particles than conventional spray drying process, improving the bioavailability of bioactive components and drugs [20].

2. Materials and methods

2.1. Materials

Preparation of unloaded and CGA-loaded nanoparticles (NPs): Maltodextrin (MD), arabic gum (AG), starch (S), carboxymethyl cellulose (CMC), hydroxypropyl methylcellulose (HPMC), Polysorbate 80 (PS80), and CGA 95 % (titration) were purchased from Sigma-Aldrich (France).

Release kinetics: the phosphate-buffered saline (PBS, pH 7.4) was prepared by mixing 80 g of sodium chloride, 2 g of potassium chloride, 17.8 g of sodium phosphate, and 2.4 g of monopotassium phosphate in distilled water to reach a final volume of 1 L. All salts were purchased from Sigma-Aldrich (France).

Biological study: Human colorectal adenocarcinoma cell lines HT-29 (ATCC® HTB-38™) and SW480 (ATCC® CCL-228™) were supplied by the American Type Culture Collection (ATCC, USA). Dulbecco's Modified Eagle Medium (DMEM), Roswell Park Memorial Institute medium (RPMI), and Fetal Bovine Serum (FBS) were sourced from Gibco (Thermo Fisher Scientific, USA). Lastly, 3-(4,5-dimethylthiazol-2-yl)-2,5-diphenyltetrazolium bromide (MTT) was purchased from Sigma-Aldrich (USA), and isopropyl alcohol from Merck (Germany).

2.2. Nanoencapsulation by spray drying

CGA-loaded nanoparticles (NPs) were produced using the laboratory-scale Nano Spray Dryer B-90 HP (Büchi Labortechnik AG, Switzerland). The key process parameters were set as follows: inlet temperature = 100 °C, drying airflow = 110–115 L min^{-1}, pump rate = 25 %, and spray rate = 80 %.

2.3. Formulations

Different feed solutions were prepared to assess their effects on the physicochemical and biological properties of CGA-encapsulated particles obtained through nanospray drying. Various biopolymeric materials were used as wall matrices for encapsulating the active molecule, including MD, AG, S, CMC, HPMC, and the surfactant PS80. Unloaded and CGA-loaded NPs were produced from aqueous feed solutions containing the wall materials alone and the wall materials combined with CGA, respectively. The CGA-loaded NPs were prepared at a 2:1 wall material-to-CGA ratio.

Formulations numbered F1-F5 (Table 1) were prepared at a feed solution concentration of 1 mg/mL. Formulations F6-F8 were prepared at a lower concentration of 0.25 mg/mL because of the high viscosity of cellulose-containing solutions, which caused atomization difficulties during nanospray drying. In addition, formulation F5 included PS80 as a surfactant at a concentration of 0.05 % (w/v).

2.4. Physicochemical characterization of nanoparticles

2.4.1. Thermal behavior

The thermal behavior of the NPs was analyzed using a thermogravimetric analyzer/differential scanning calorimeter (TGA/DSC, Mettler Toledo). Samples were placed in a 60 μL platinum pan and heated from 25 to 800 °C at 10 °C/min under an inert nitrogen atmosphere.

2.4.2. Chemical composition

The chemical composition of the NPs was determined by Fourier transform infrared (FTIR) spectroscopy using a Nicolet 6700 FTIR spectrophotometer (Thermo Fisher Scientific) equipped with an attenuated total reflectance (ATR) accessory. Powder samples were positioned on the ATR crystal, and spectra were recorded in the 4000–400 cm^{-1} range, with 16 successive scans per sample at a resolution of 4 cm^{-1}.

2.4.3. Morphology and particle size

The morphology and surface characteristics of the NPs were examined by Field-Emission Scanning Electron Microscopy (FE-SEM, JSM 7100F, JEOL). Samples were placed on carbon conductive adhesive tabs and coated with a thin layer of gold using a plasma coater. The samples were scanned by detecting secondary electrons at an acceleration of 10 kV and a magnification of 16,000 × .

2.4.4. Release kinetics

The sample-and-separate method was used to evaluate the release profiles of the different formulations in PBS (pH 7.4) maintained at 38 ± 2 °C. Samples were collected at various time points up to 360 min, when maximum release was achieved for all formulations. Each sample was filtered through a PTFE syringe filter (0.22 μm pore size), and the absorbance was measured using a UV–Vis spectrophotometer (UV-1800, Shimadzu) at 325 nm. All release profiles were performed in triplicate.

The encapsulation efficiency (EE = weight of CGA encapsulated in NPs/weight of CGA in feed solution × 100) and the drug loading content (DLC = weight of CGA encapsulated in NPs/weight of NPs × 100) were calculated based on the final values of released CGA.

2.5. Biological tests

2.5.1. Cell culture

Human colorectal adenocarcinoma cell lines HT-29 and SW480 were

Table 1
Composition of unloaded nanoparticle formulations.

Formulation	Wall Materials	Wall materials ratio
F1	Maltodextrin	1
F2	Maltodextrin + Arabic Gum	1:1
F3	Arabic Gum	1
F4	Maltodextrin + Starch	1:3
F5	Maltodextrin + Arabic Gum + PS80	1:1
F6	Carboxymethyl cellulose	1
F7	Hydroxypropyl methylcellulose	1
F8	Carboxymethyl cellulose + Hydroxypropyl methylcellulose	1:1

employed in this study. Cells were cultured in a humidified atmosphere at 37 °C with 5 % CO_2. Culture media and supplements were added according to the manufacturer's instructions.

2.5.2. Treatments conditions

All nanoparticulate powder formulations (F1–F8) were dispersed in 1000 μL of fresh culture medium, and the corresponding dilutions were prepared to obtain equivalent CGA concentrations of 10, 100, 500, and 1000 μM for unloaded NPs. For CGA-loaded NPs, concentrations of 50, 100, 200, and 400 μM were selected based on the results obtained for the unloaded formulations (see Section 3.2.1.1).

2.5.3. Cytotoxicity and proliferation assay (MTT)

The MTT assay was used to evaluate the cytotoxicity of unloaded NPs and both the cytotoxicity and antiproliferative effects of CGA-loaded NPs on HT-29 and SW480 cell lines. Cells were seeded in 96-well plates at a density of 1×10^4 cells/well and incubated overnight at 37 °C. Treatments were applied for 24, 48, and 72 h, with untreated cells serving as controls. After treatment, the medium was replaced with fresh medium containing MTT (0.5 mg/mL), followed by incubation for 2 h at 37 °C. The MTT solution was then removed, and formazan crystals were dissolved in acidified isopropyl alcohol. Readings were performed at 560 nm using a Varioskan multimode microplate reader (Thermo Fisher Scientific).

Cell viability was expressed as a percentage relative to the untreated control as (absorbance of treated cells − absorbance of background controls)/(absorbance of untreated cells − absorbance of background controls) × 100. The mean inhibitory concentration (IC_{50}) for each formulation was determined by statistical approximation using GraphPad Prism 8.1 (GraphPad, USA).

2.5.4. Cell cycle analysis by flow cytometry

For cell cycle analysis, 5×10^5 cells/well were seeded in 6-well plates and treated as described above. Subsequently, cells were detached, fixed in cold 70 % ethanol, and stored at 4 °C. Permeabilized cells were treated with 100 μg/mL RNase (R5000, Sigma-Aldrich, USA) and stained with 100 μg/mL propidium iodide (P4170, Sigma-Aldrich, USA) for 30 min. Samples were analyzed by flow cytometry (BD LSR Fortessa; BD Biosciences, USA), and data were processed using FlowJo software (FlowJo LLC, USA).

2.5.5. Hoechst 33342 staining for apoptosis detection

Apoptosis in SW480 and HT-29 cells was quantified by Hoechst 33342 staining (Thermo Fisher Scientific, USA). Cells were seeded in a 24-well plate at a density of 2.5×10^5 cells/mL and cultured under standard conditions for 24 h. After treatment with the different formulations, the culture medium was removed and cells were washed with PBS (Gibco, USA) and incubated with 50 μL of Hoechst 33342 at room temperature for 5 min. Apoptotic cells were visualized by fluorescence microscopy using a Nikon Eclipse Ti inverted microscope (Nikon, Japan). The apoptotic index was calculated as the number of apoptotic cells/total number of cells × 100. All biological tests were conducted in triplicate. Results are expressed as the mean ± standard error of the mean from three independent experiments.

3. Results

3.1. Physicochemical characterization of the nanoparticles

Unloaded and CGA-loaded NPs were obtained from different feed formulations varying in wall materials and their proportions, as shown in Table 1.

3.1.1. Thermal behavior

The thermal behavior of the different NPs was analyzed. Although results for all formulations are not shown, F3 and F8 were selected as representative examples. Formulation F3 represents non-cellulosic polysaccharide-based wall materials (F1–F5), whereas F8 represents cellulose-based formulations (F6–F8). Therefore, this section presents the results for unloaded and CGA-loaded F3 and F8 NPs (Fig. 1a and b). In each figure, continuous lines correspond to unloaded NPs and the active CGA molecule, while dashed lines represent CGA-loaded NPs.

The pure CGA molecule exhibited a 3 % mass loss between 25 and 150 °C, associated with water evaporation. A further 7 % loss between 190 and 260 °C was attributed to melting-crystallization of the molecule [21]. The main degradation occurred between 260 and 460 °C, corresponding to a 62 % mass loss, with the highest rate at 320–350 °C, related to CGA decomposition [22]. The final residue of CGA was 28 %.

The TGA thermograms of the unloaded formulations F3 (AG) and F8 (CMC + HPMC) showed an initial mass loss between 30 and 160 °C, related to water evaporation of approximately 10 % and 7 %, respectively. For the unloaded AG NPs (Fig. 1a), the main 71 % mass loss occurred between 160 and 390 °C, attributed to material depolymerization. A secondary 13 % loss was observed between 620 and 800 °C due to AG decomposition, leaving a 6 % residue that indicates incomplete biopolymer decomposition.

Similarly, the unloaded CMC + HPMC NPs (Fig. 1b) displayed multiple mass-loss stages. After water evaporation, a main 53 % loss occurred between 160 and 390 °C, associated with depolymerization of carboxymethyl cellulose and hydroxypropyl methylcellulose, with maximum loss at 300 °C. This was followed by a gradual 10 % loss between 390 and 600 °C, suggesting further degradation of HPMC, which appears to decompose at slightly higher temperatures than CMC [23]. Between 600 and 800 °C, an additional 12 % loss was observed, leaving a 6 % residue that confirms incomplete decomposition of both cellulose derivatives.

For both formulations, the thermograms of the CGA-loaded NPs (dashed lines) initially resembled those of their respective wall materials until approximately 300 °C for F3 and 350 °C for F8. Beyond these temperatures, the profiles became similar to that of pure CGA, suggesting that CGA was effectively encapsulated within the wall materials. The CGA-loaded NPs exhibited excellent thermal stability.

3.1.2. Chemical composition

FTIR spectroscopy was performed to verify the presence and structural characteristics of the molecular constituents in the NPs. Spectra of all formulations were analyzed; however, only the results for F3 and F8 are presented here, as they are representative of the non-cellulosic polysaccharide-based (F1–F5) and cellulose-based (F6–F8) formulations, respectively. The other formulations exhibited similar spectral behavior.

The spectrum of F3 unloaded (AG) NPs (Fig. 2a) displayed a broad stretching band at 3350 cm^{-1} corresponding to hydroxyl (—OH) groups. Absorption bands at 2930 cm^{-1}, 1606 cm^{-1}, 1420 cm^{-1}, and in the 1025–770 cm^{-1} range were attributed to vibrational modes of C—H groups, —COOH (carboxylic groups), and C—O, C—C, and C—O—C stretching, as well as C—O—H and C—H bending modes of the AG polymer backbone [24].

The F8 unloaded (CMC + HPMC) NPs (Fig. 2b) exhibited absorption bands at 3395 cm^{-1} for hydroxyl (—OH) groups, 2907 cm^{-1} for C—H stretching from CH_2 groups, and 1592 cm^{-1} and 1412 cm^{-1} for stretching of carboxylate groups ($—COO^-$). Bands at 1322 cm^{-1}, 1264 cm^{-1}, and 1058 cm^{-1} correspond to O—H bending and C—O and C—O—C stretching vibrations, respectively. The band at 895 cm^{-1} is attributed to β-glycosidic linkages between glucose units in the cellulose backbone, which are preserved in CMC [25].

The CGA spectrum exhibited a characteristic absorption band at 3323 cm^{-1} corresponding to hydroxyl (—OH) groups. The band observed at 1685 cm^{-1} was attributed to C=O stretching vibrations of the ester carbonyl group. Additional bands at 1638 cm^{-1}, 1600 cm^{-1}, and 1520 cm^{-1} are linked to C=C stretching vibrations in the aromatic ring.

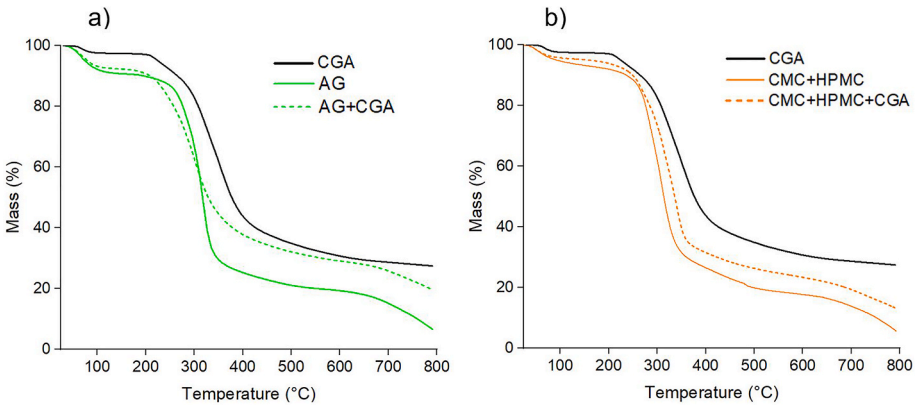

Fig. 1. TGA thermograms of (a) F3 (AG); (b) F8 unloaded (CMC + HPMC) (continuous line) and CGA-loaded (dashed line) nanoparticles.

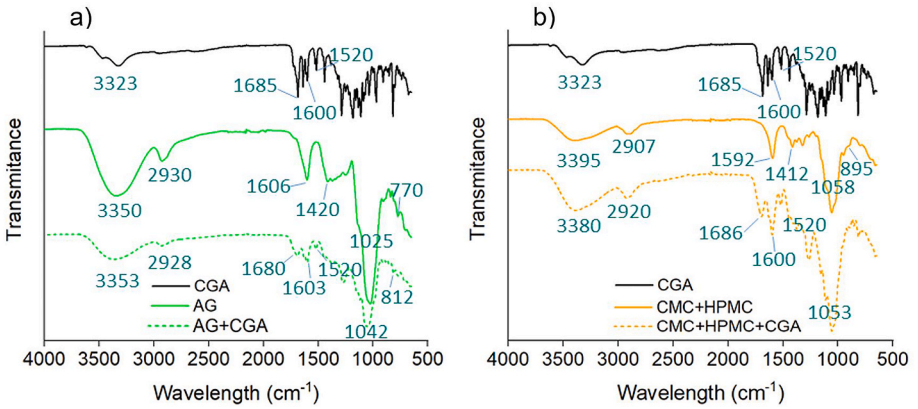

Fig. 2. FTIR spectra of (a) CGA, F3 unloaded (AG), and F3 CGA-loaded nanoparticles; (b) CGA, F8 unloaded (CMC + HPMC), and F8 CGA-loaded nanoparticles.

The spectra of the CGA-loaded formulations F3 (AG + CGA) (Fig. 2a) and F8 (CMC + HPMC + CGA) (Fig. 2b), also exhibited the broad band of hydroxyl (—OH) groups at 3353 cm^{-1} and 3380 cm^{-1}, respectively. Bands at 2928 cm^{-1} and 2920 cm^{-1} correspond to C—H stretching vibrations of CH_2 groups, characteristic of the wall materials AG and CMC + HPMC, respectively. The presence of CGA in each sample was confirmed by the bands at 1680 cm^{-1} and 1686 cm^{-1} for F3 and F8 formulations, respectively, which correspond to the C=O stretching vibrations of the ester carbonyl group, and by the bands at 1600 cm^{-1} and 1520 cm^{-1}, associated with C=C stretching vibrations in the aromatic ring of CGA.

These results demonstrate that the NPs produced contain both the wall materials and CGA, supporting that chlorogenic acid was successfully encapsulated within the different wall matrices as expected.

3.1.3. Morphology and particle size

The morphology of unloaded and CGA-loaded NPs from the different formulations was analyzed by FE-SEM. Representative micrographs of F3 and F8 unloaded formulations are shown in Fig. 3a–b, and those of F3 and F8 CGA-loaded formulations in Fig. 3c–d.

Images of both unloaded and CGA-loaded NPs from formulations F1-F5 exhibited similar morphology and particle size, regardless of the different wall materials used. As shown in Fig. 3a and c for F3, the NPs predominantly displayed spherical and smooth morphology, with a mean number diameter of approximately $d_n = 360$ nm (determined by measuring over 300 NPs using ImageJ software). Slight shell buckling was occasionally observed.

In contrast, NPs from formulations F6–F8 presented moderately smaller sizes, attributable to the lower concentration (0.25 mg/mL) of the feed solution used in the cellulose-based formulations. As illustrated

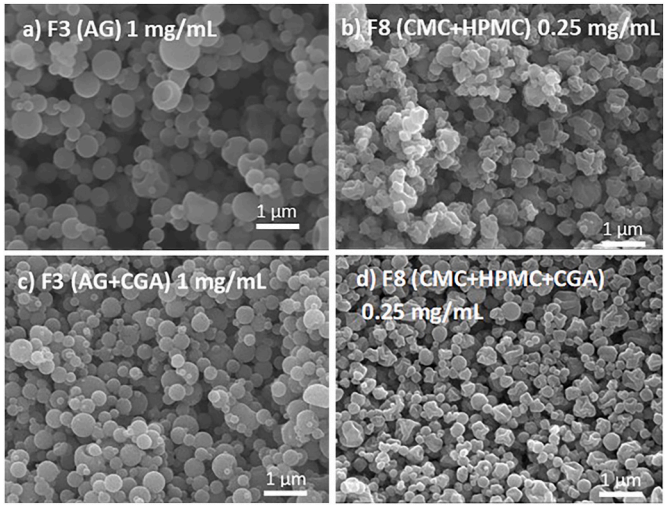

Fig. 3. FE-SEM micrographs of (a) F3 unloaded nanoparticles; (b) F8 unloaded nanoparticles; (c) F3 CGA-loaded nanoparticles; (d) F8 CGA-loaded nanoparticles.

for F8 (CMC + HPMC) in Fig. 3b and d, the NPs appear wrinkled, likely due to folding of the early crust formed during the particle drying process [26]. The mean number diameter for these particles was approximately $d_n = 251$ nm.

The active ingredient appears to be well integrated within the wall materials, as no distinct CGA clusters were observed. This suggests successful encapsulation of CGA within the various biopolymer carriers.

3.1.4. Release kinetics

The sample-and-separate method was employed to assess the release profiles of the CGA-loaded NPs and to determine the possible impact of the wall material on CGA release. Formulations F1 (MD + CGA), F2 (MD + AG + CGA), F3 (AG + CGA), and F6 (CMC + CGA) were analyzed. F6 represents cellulose-based formulations, whereas the other three samples are representative of MD- and AG-based systems. The analysis of F2 was done to evaluate whether combining wall materials produced any synergistic effects on CGA release kinetics.

As shown in Fig. 4, NPs prepared with MD, AG, or their combination exhibited an almost instantaneous CGA release, reaching 100 % within a few seconds. This behavior is attributed to the high solubility of MD (up to 240 % w/v) and AG (up to 50 % w/v) in aqueous media. In contrast, CMC-based NPs displayed slower kinetics, achieving 80 % CGA release after 10 min and complete release after 360 min. Thus, cellulose-based formulations, such as F6, provide an extended CGA release.

EE and DLC were calculated for the four formulations (Table 2). The results were similar across formulations, showing high EE values that indicate minimal CGA loss during encapsulation. The DLC values were consistent with the 2:1 wall material-to-CGA ratio used in the feed formulations, confirming that the NPs contained the expected CGA amount.

3.2. Biological tests

3.2.1. Cell viability and proliferation assays

3.2.1.1. Cytotoxicity of wall materials. The cytotoxicity of the wall materials was first evaluated using the MTT assay (Fig. 5). According to ISO 10993–5:2009, a material is considered cytotoxic when cell viability falls below 70 %. In the present study, cell viability for formulations F2-F8 remained above this threshold in both SW480 and HT-29 cell lines, confirming their biocompatibility across all tested concentrations. In contrast, F1 exhibited a slight reduction in viability in SW480 cells at the highest concentration tested. These results suggest that the materials used for nanoencapsulation are non-cytotoxic in the evaluated cell lines, except for those in formulation F1 at 500 μM.

Since unloaded NPs showed no cytotoxicity across all formulations at concentrations below 500 μM, the maximum concentration selected for subsequent experiments was 400 μM.

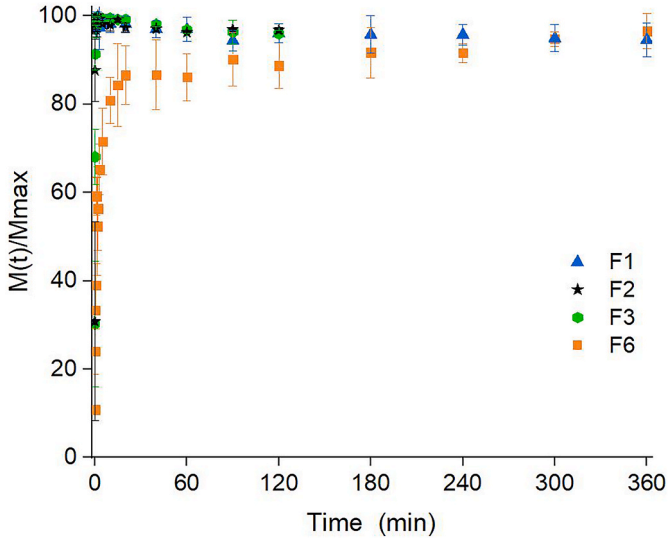

Fig. 4. Release kinetics of CGA-loaded nanoparticles: F1 (MD + CGA), F2 (MD + AG + CGA), F3 (AG + CGA), and F6 (CMC + CGA). *M*(*t*): CGA mass released at time *t*; *Mmax*: maximum CGA mass released during the experiment. Mean values and error bars correspond to triplicate experiments.

Table 2
Encapsulation efficiency and drug loading content for F1, F2, F3, and F6 formulations. Mean values and standard deviations correspond to triplicate experiments.

Formulation	EE (%)	DLC (%)
F1	112.8 ± 5.0	37.6 ± 1.7
F2	113.4 ± 8.5	37.8 ± 2.8
F3	101.3 ± 2.2	33.8 ± 0.7
F6	109.8 ± 7.3	36.6 ± 2.43

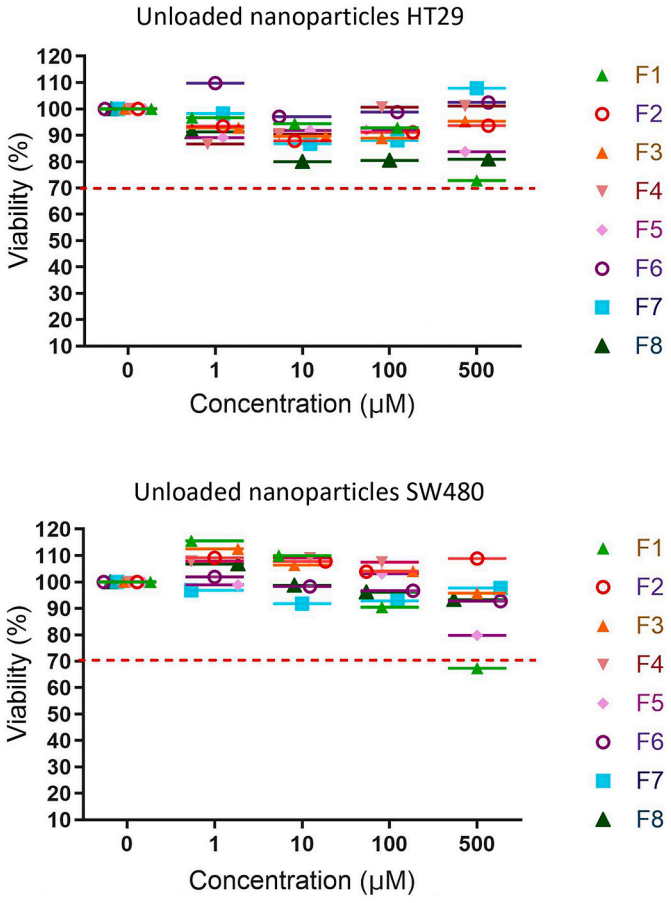

Fig. 5. Cytotoxicity (% viability) of unloaded nanoparticles. Values are expressed as mean ± standard error of the mean from three independent experiments.

3.2.1.2. Cytotoxicity of the natural compound (CGA). The cytotoxic effects of CGA-loaded formulations F1–F8 were evaluated in SW480 and HT-29 cell lines. Fig. 6 shows the results for each formulation at four concentrations (50, 100, 200, and 400 μM) after 24 and 48 h of treatment. Free CGA was used as the control at the same concentrations.

CGA-loaded formulations exhibited low cytotoxicity, although significant differences were observed between cell lines. In SW480 cells, a moderate decrease in viability was detected after 24 h across all formulations and concentrations. However, after 48 h, viability generally returned to baseline, except for formulations F6–F8, which maintained a modest reduction.

In HT-29 cells, a similar trend was noted, although overall viability was consistently lower compared to SW480 cells for formulations F1-F5. Notably, formulations F1 and F3 induced significant reductions in viability at 100 μM (F1) and at both 100 and 200 μM (F3). After 48 h, this effect persisted only for F1, while the remaining formulations continued to display minimal cytotoxicity.

Additionally, IC_{50} values were calculated for each treatment.

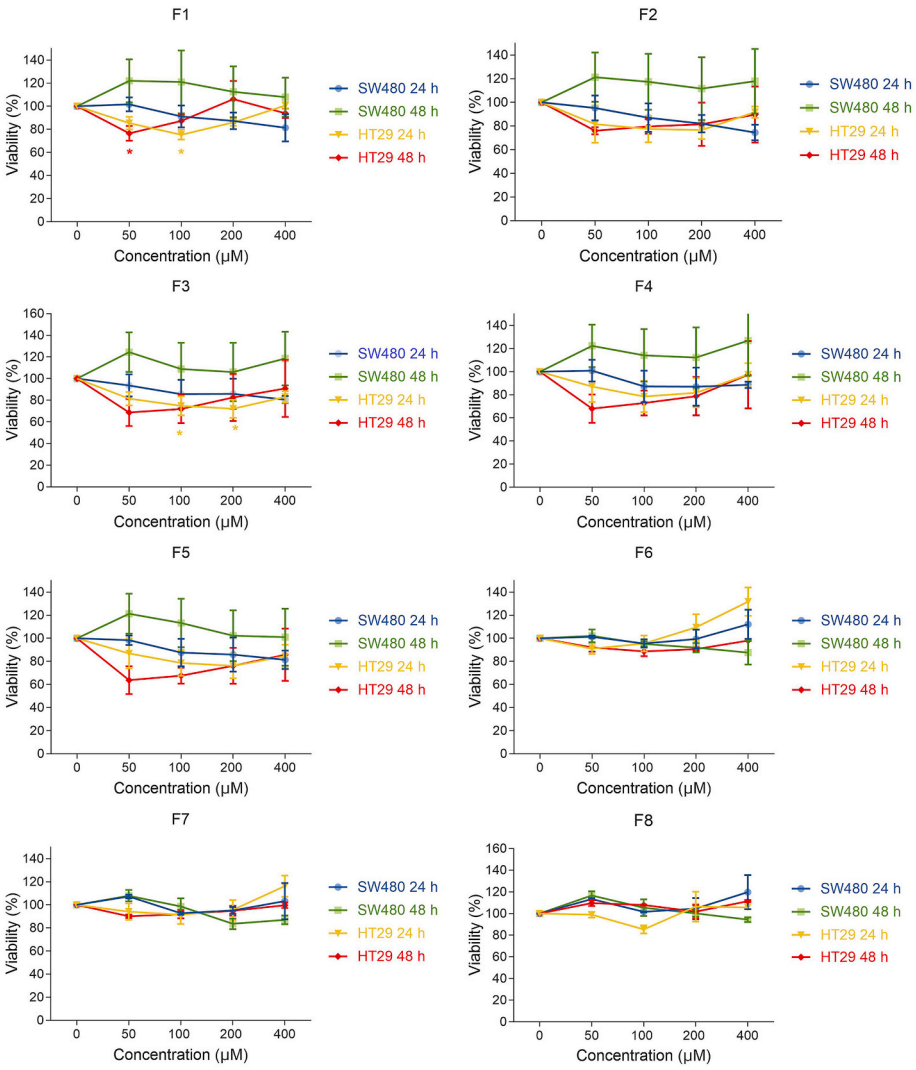

Fig. 6. Cytotoxicity (% viability) of CGA-loaded nanoparticles. Values are expressed as mean ± standard error of the mean from three independent experiments.

Interestingly, the AG + CGA formulation (F3) exhibited the lowest IC_{50} values in HT-29 cells, with 759 and 678 μM after 24 and 48 h of treatment, respectively.

HT-29 cells were more sensitive to CGA-loaded formulations than SW480 cells. Although none of the treatments produced significant cytotoxic effects at concentrations up to 400 μM, F1 and F3 demonstrated the strongest biological activity, particularly in HT-29 cells. Conversely, free CGA tended to reduce cell viability more markedly in SW480 cells than in HT-29 cells under the same experimental conditions.

3.2.1.3. Proliferation in SW480 and HT-29 cells (MTT assay). The proliferative response of SW480 and HT-29 cell lines was evaluated following treatment with CGA-loaded NPs at concentrations of 50, 100, 200, and 400 μM. Results, presented in Fig. 7, were compared with those of untreated controls and cells treated with free CGA. Measurements were performed at 24, 48, and 72 h for both cell lines.

In the SW480 cell line, treatment with free CGA did not affect proliferative capacity at 24 and 48 h for concentrations between 50 and 200 μM, although a slight decrease was observed at 72 h compared with untreated cells. At the highest concentration (400 μM), a significant and time-dependent reduction in proliferation was detected. F1 induced a decrease in proliferation across concentrations and time points, except at 50 μM after 24 h, where an increase in cell number was observed. The greatest inhibitory effect for F1 occurred at 200 and 400 μM. Formulations F2–F5 produced similar results, with a significant, time-dependent reduction in proliferation compared to untreated controls. In contrast, formulations F6–F8, based on cellulose products, displayed a different behavior, allowing sustained cell growth. Only at higher concentrations (200 and 400 μM) was growth inhibition evident.

In HT-29 cells, free CGA induced a decrease in proliferation at 50 and 100 μM after 48 and 24 h, respectively. CGA-loaded formulations F1 and F4 further reduced proliferation at these concentrations and time points. The strongest inhibitory responses for formulations F2 and F3 were observed at 50 and 100 μM after 24 and 48 h. For its part, F5 produced the greatest reduction at 50 and 200 μM after 48 and 24 h, respectively. Conversely, cellulose-based formulations F6-F8 did not significantly affect HT-29 proliferation capacity at 24 and 48 h.

Overall, these findings indicate that specific formulations may induce a decrease in the proliferative capacity of SW480 and HT-29 cells, with F1, F2 and F3 showing the most pronounced effects. In the HT-29 line, formulations F2 and F3 reached significant population decreases at concentrations as low as 50 μM after 48 h. The results suggest a potential cytostatic activity of these formulations, particularly on HT-29 cells, which have previously been reported to exhibit higher resistance to CGA at comparable doses [9].

3.2.1.4. Cell cycle distribution in HT-29 cells. Cell cycle distribution

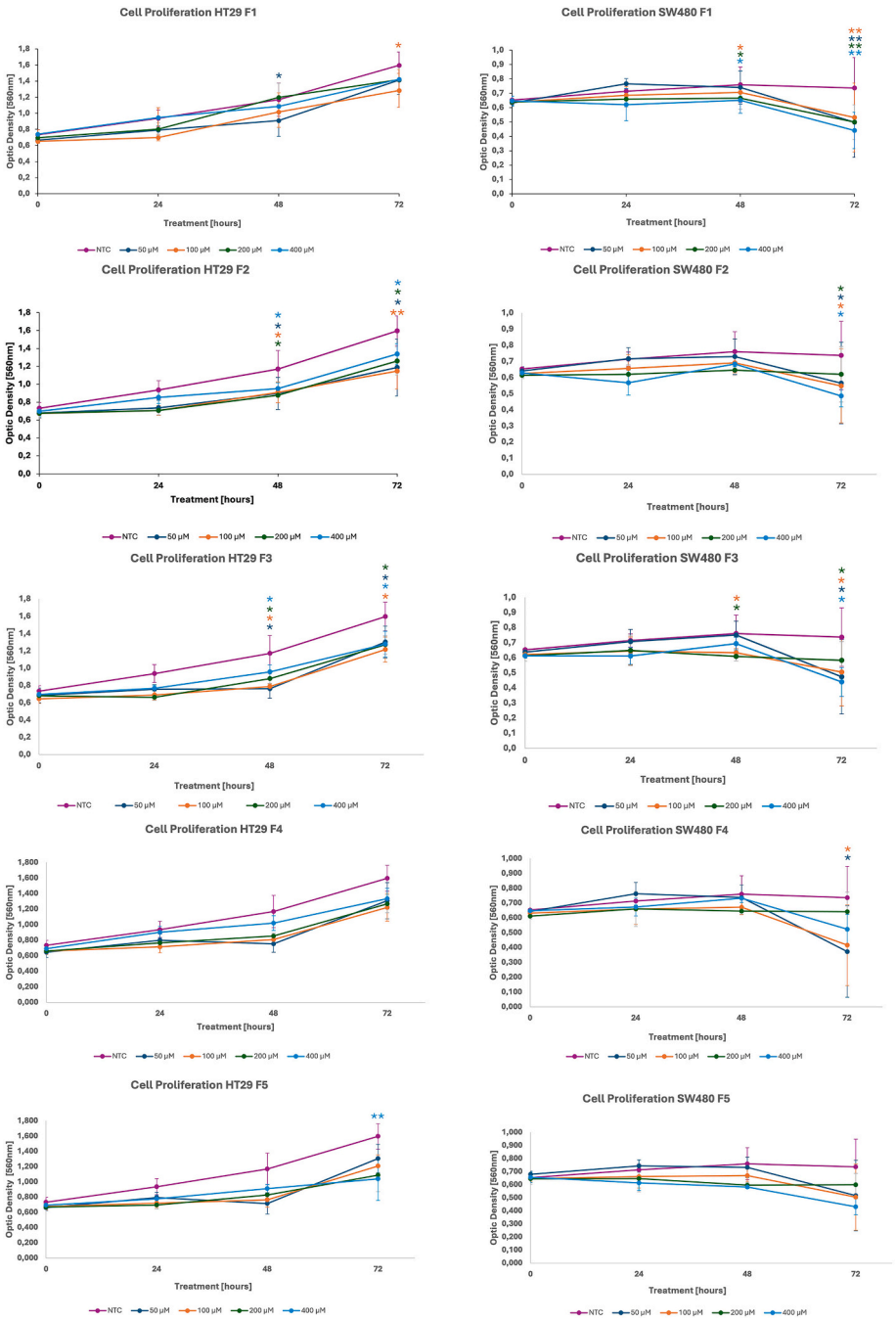

Fig. 7. Cell proliferation in SW480 and HT-29 cell lines treated with free CGA and CGA-loaded formulations at four concentrations. Values are expressed as mean ± standard error of the mean from three independent experiments.

analysis was performed to evaluate the effects of formulations F1 and F3 on HT-29 cells after 48 h of exposure (Fig. 8). Untreated cells showed a typical profile, with most cells residing in the G1 phase. Treatment with either F1 or F3 resulted in a slight but consistent increase in the sub-G1 population, accompanied by a decrease in the proportion of G1 phase cells compared with untreated controls. Beyond these shared effects, F1-treated cells exhibited an increase in S phase and a reduction in the G2/M fraction, whereas F3-treated cells displayed an accumulation in G2/M without a noticeable rise in S phase. These results suggest that F1 primarily affects S phase progression, while F3 induces changes leading to G2/M accumulation.

No statistically significant differences were found between treatments; however, consistent trends were observed, including a modest increase in the sub-G1 fraction and a decrease in G1 for both formulations, an increase in S phase for F1, and a G2/M accumulation for F3.

3.2.2. *Possible cell death mechanism: apoptosis*

Given the cytotoxic effects observed in cells treated with CGA-loaded NPs using formulations F1, F2 and F3, a Hoechst 33342 staining assay was carried out to determine whether cell death was linked to apoptosis. Cells were treated under different conditions and subsequently examined using fluorescence microscopy.

As shown in Fig. 9, SW480 and HT-29 cells exposed to CGA-loaded

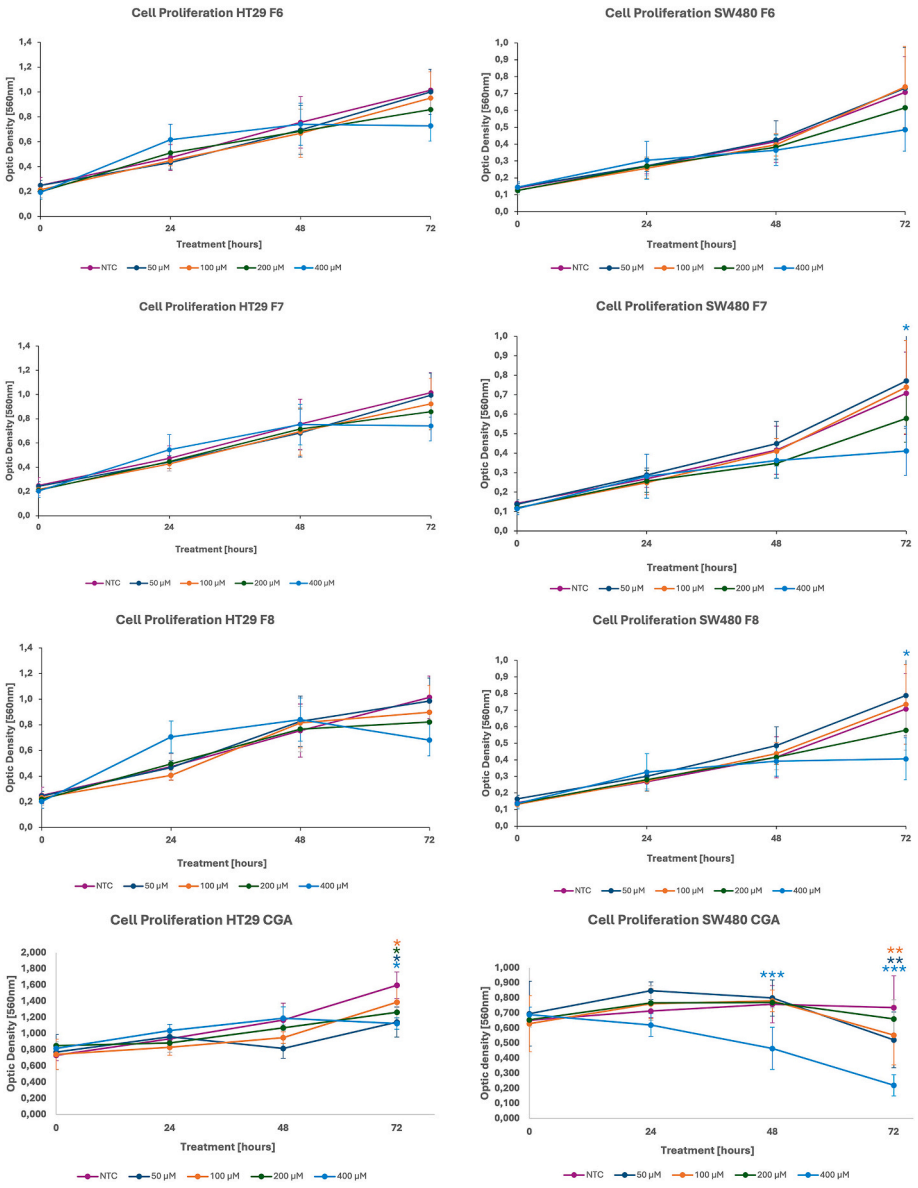

Fig. 7. (*continued*).

NPs (formulations F1 and F3, 200 µM) exhibited no significant increase in apoptotic nuclei. In SW480 cells, the percentage of apoptotic nuclei was approximately 3.5 % in the control and remained near 2 % after treatment with F1 or F3. In HT-29 cells, apoptosis levels were around 2 % in the control and showed no relevant changes upon treatment with either formulation. Overall, no statistically significant differences were observed between control and experimental conditions.

4. Discussion

The anticancer activity was notably enhanced by CGA-loaded NPs in formulations F1-F3 compared with free CGA. Interestingly, this enhancement was not limited to the formulations containing AG (F2 and F3). The observed effect could be attributed to the small particle size, which improves bioavailability and promotes cellular uptake. The high solubility of AG and the ease with which the composite traverses the cell membrane may enable more efficient internalization of the drug, thereby improving cytotoxicity in the AG + CGA formulation [27].While greater bioavailability due to small particle size likely contributes to this effect, the enhanced activity cannot be explained solely by release kinetics, as F1 (MD) exhibited a rapid release profile similar to F2 and F3 (both AG-based).

Although MD per se is considered inert, certain resistant forms have demonstrated antitumor effects in CRC models by inducing apoptosis (via ROS, Bax, caspases, and Akt/mTOR signaling) and inhibiting tumor growth *in vivo* [28,29]. Moreover, the intrinsic composition of AG may influence the biological behavior of the formulations, as this natural exudate contains not only polysaccharides but also proteins, which could modulate NP-cell interactions, uptake, and intracellular responses. AG has shown antiproliferative activity in triple-negative breast cancer cells through G1/S arrest, apoptosis induction, and suppression of Wnt/β-catenin signaling [30]. Furthermore, it has been reported to reduce tumor volume in animal models and to potentiate apoptotic responses when used to stabilize NP systems [31,32].

The evaluation of all CGA-loaded NP formulations revealed low overall cytotoxicity in both SW480 and HT-29 CRC cell lines, with differential responses depending on cell line and treatment duration. In SW480 cells, a transient reduction in viability was observed after 24 h for all formulations and concentrations; however, this effect diminished by 48 h in most cases. This response may be explained by the rapid

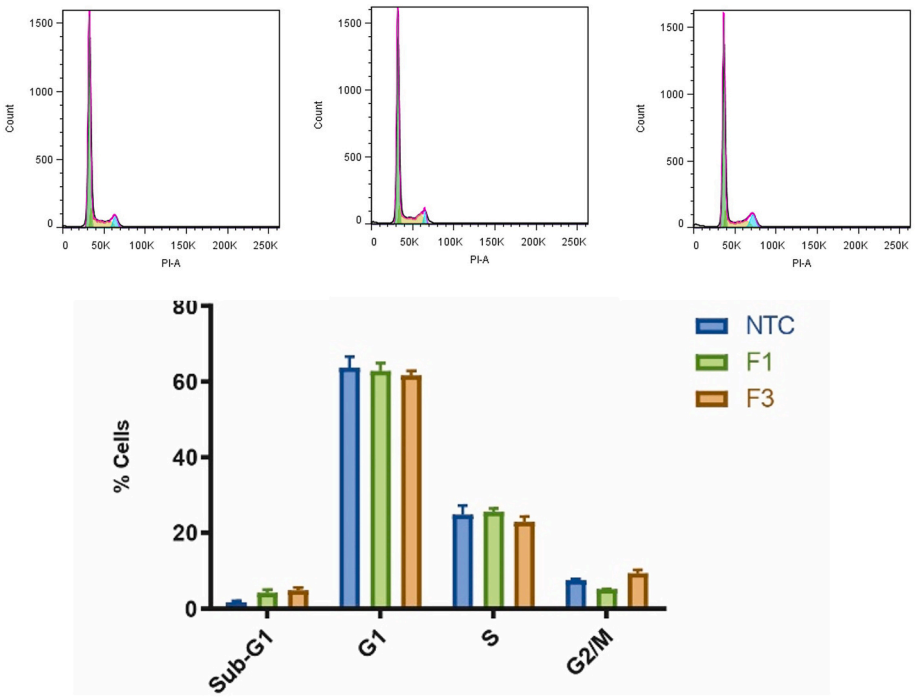

Fig. 8. Cell cycle distribution of HT-29 cells after 48 h of treatment with F1 or F3. (a) Representative DNA content histograms obtained by flow cytometry for untreated cells (NTC), and for cells treated with F1 or F3. Peaks corresponding to sub-G1, G1, S, and G2/M phases are indicated. (b) Quantitative analysis of the percentage of cells in each cell cycle phase under the three experimental conditions. Values are expressed as mean ± standard deviation from three independent experiments.

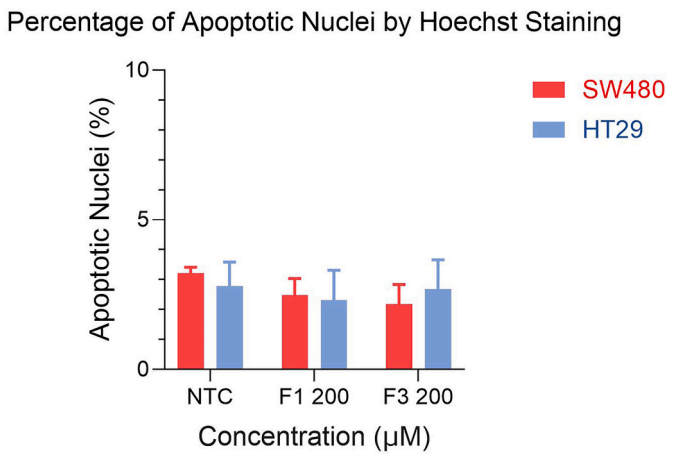

Fig. 9. Apoptosis detected by Hoechst 33342 staining. SW480 and HT-29 cells were exposed to formulations F1 and F3 at 200 μM. Data are expressed as mean ± standard deviation from three independent experiments.

release and subsequent metabolism of CGA from NPs, resulting in lower bioavailability throughout the treatment period. Similar results were reported by Evans et al. [33], who demonstrated that several anticancer agents exhibit early cytotoxic effects that diminish after 48 h due to compound instability or metabolism in the culture medium.

Despite this trend, formulations F6, F7, and F8 maintained a slight reduction in cell viability after 48 h of treatment, which could be interpreted as slower release profile or greater stability of the CGA encapsulated in these specific formulations. Comparable findings have been reported for NP systems that extend the biological activity of polyphenols by modulating release kinetics or improving compound stability in biological environments [34].

In HT-29 cells, increased sensitivity to CGA-loaded formulations was observed, as indicated by consistently lower viability values compared to SW480 cells. Among the tested systems, F1 and F3 exhibited the strongest antiproliferative effects at concentrations of 100 and 200 μM, particularly at earlier time points. Notably, only F1 retained this effect after 48 h, highlighting the variability in release kinetics and cellular responses among NP systems. These findings are consistent with previous studies showing that cell line-specific characteristics such as membrane composition, antioxidant capacity, and metabolic profile significantly influence cellular responses to polyphenolic compounds like CGA [35,36].

Overall, HT-29 cells were more susceptible to treatment with CGA-loaded formulations in terms of both cytotoxicity and inhibition of proliferation. Interestingly, earlier reports have indicated that SW480 cells are typically more sensitive to CGA, primarily due to its capacity to modulate the Wnt/β-catenin signaling pathway, a key regulator of CRC progression [9]. Consistent with these findings, free CGA, used as a control in this study, elicited a stronger cytotoxic response in SW480 than in HT-29 cells. However, encapsulation altered this pattern, suggesting that nanoencapsulation modifies CGA's cellular uptake, distribution, or bioavailability. Indeed, the pharmacokinetics of polyphenols, including CGA, are known to change substantially after nanoencapsulation, which influences their internalization, stability, and retention within target cells [37].

HT-29 cells, characterized by high expression of detoxification and transport proteins, may particularly benefit from encapsulation strategies that facilitate compound passage across membranes and thereby improve intracellular retention. Elevated levels of breast cancer resistance protein (BCRP) have been reported in HT-29 cells. BCRP functions as an efflux pump with broad substrate specificity, promoting the detoxification and expulsion of therapeutic agents [38]. Similarly, variable levels of UDP-glucuronosyltransferases (UGTs) have been described in CRC cells. UGTs catalyze glucuronidation reactions that facilitate the elimination of xenobiotics, including phenolic compounds. High UGT activity has been associated with reduced drug bioavailability, premature glucuronidation, and diminished therapeutic

efficacy. Notably, several UGT1A isoforms are overexpressed in HT-29 cells [39].

Encapsulation of anticancer agents within nanocarriers has proven effective in mitigating tumor resistance by circumventing drug-efflux systems and attenuating detoxification pathways. Carriers that enter cells predominantly via endocytosis or enhance membrane translocation improve intracellular and nuclear drug retention in P-gp/ABCB1-overexpressing models, consequently restoring antitumor activity relative to free drugs. Furthermore, pH-sensitive conjugates promote lysosomal release and prolong drug persistence in resistant cells [40]. Likewise, biomimetic "tea" NPs have been shown to bypass ABCB1-mediated efflux and increase doxorubicin accumulation in SW620/Ad300 CRC cells [41]. Beyond optimizing transport, micellar systems incorporating glutathione S-transferase (GST) inhibitors reduce detoxification capacity and reverse cisplatin resistance [42].

In this study, cell cycle analysis was performed exclusively on HT-29 cells, as this line exhibited superior biological activity in prior assays. The analysis was limited to formulations F1 and F3, given their stronger responses. The evaluation was conducted at 48 h, using the lowest concentration that had induced biological activity. Although no statistically significant differences were observed, both formulations induced a slight increase in the sub-G1 fraction and a decrease in G1-phase cells relative to untreated controls. Beyond these shared effects, F1-treated cells accumulated in the S phase, while F3-treated cells showed enrichment in G2/M. Together with the absence of apoptotic nuclear morphology and stable cell viability under identical conditions, these findings support the conclusion that F1 and F3 primarily exert cytostatic rather than cytotoxic effects, likely through modulation of cell cycle progression.

CGA has consistently been reported to exert cytostatic activity in CRC models, largely through modulation of cell cycle progression. In HT-29 and HCT-116 cells, CGA induces S-phase arrest, likely mediated by disruption of the ERK signaling pathway [43]. This phase-specific blockade aligns with findings in Caco-2 cells, where CGA and its microbial metabolites (e.g., caffeic acid, 3-phenylpropionic acid, benzoic acid) cause S-phase arrest, particularly at lower synergistic concentrations, supporting their role in inhibiting proliferation without necessarily invoking apoptosis. Moreover, broader reviews have confirmed that CGA and related compounds reduce viability across multiple CRC lines, including HT-29, mainly through cytostatic mechanisms such as cell cycle arrest, Wnt/β-catenin modulation, and ROS induction, rather than direct cytotoxicity [44]. Collectively, these findings reinforce the interpretation that CGA's antiproliferative effects are primarily mediated by disruption of cell cycle progression, corroborating our observations for F1 and F3 in HT-29 cells.

To determine whether the observed reduction in cell viability induced by CGA-loaded formulations was associated with apoptotic mechanisms, a Hoechst staining assay was performed. Treatment with formulations F1 and F3 did not increase nuclear condensation or fragmentation—hallmarks of apoptosis [45]—in either SW480 or HT-29 cells. However, a dose-dependent decrease in the percentage of apoptotic nuclei was observed for both formulations. These results suggest that the cytotoxic and antiproliferative effects previously observed with F1 and F3 are not primarily mediated by apoptosis. Instead, they likely involve alternative mechanisms such as cell cycle arrest or cytostatic effects [46], especially in the HT-29 cell line.

These findings highlight the critical role of both formulation design and treatment duration in optimizing the therapeutic efficacy of CGA-based nanoformulations. Moreover, they emphasize the need to account for controlled-release behavior in extended *in vitro* assays, as early cytotoxic effects may not accurately reflect long-term cellular responses if the active compound undergoes rapid degradation or metabolism in the culture medium.

Recent advances in nanotechnology for cancer treatment have focused on the design of biocompatible, surface-modified, and stimulus-responsive nanocarriers that enhance drug delivery and therapeutic outcomes [47]. The present study is promising and opens avenues for improving the performance of CGA-loaded nanocarriers. Future research should aim to develop surface-modified, spray-dried loaded NPs capable of controlling and extending CGA release, followed by in-depth studies of their interactions with biological systems to achieve improved targeting. Furthermore, the challenge of securing effective intestinal absorption via oral administration remains a critical obstacle for positioning NPs as a viable CRC therapeutic option [18,48].

5. Conclusions

The results demonstrate that the nanoencapsulation of CGA, particularly in formulations F1-F3, enhances its antiproliferative potential in CRC cells compared with the free compound. While classical apoptotic pathways do not appear to be the primary mechanism, cell cycle analysis revealed trends consistent with cytostatic effects, including a slight rise in the sub-G1 fraction and a decrease in the G1 fraction for both formulations, an increase in S phase for F1, and an accumulation in G2/M for F3. Although these differences were not statistically significant, they suggest that cell cycle arrest may contribute to the observed antiproliferative activity. Further complementary experiments will be necessary to confirm this hypothesis.

These findings underscore the importance of formulation composition, particle size, and bioavailability in modulating cellular responses and support the development of CGA-based nanocarriers as promising candidates for CRC treatment. Furthermore, the results highlight the need to consider both treatment duration and compound stability when evaluating *in vitro* anticancer potential. While CGA-loaded formulations initially exhibited cytotoxic activity, these effects were transient in several cases, likely due to compound degradation or metabolism. Nonetheless, certain formulations, such as F6–F8, maintained moderate activity over time, suggesting slow release kinetics.

CRediT authorship contribution statement

Daniel Tobón-Vélez: Writing – review & editing, Writing – original draft, Visualization, Investigation, Conceptualization. **Mallorie Tourbin:** Writing – review & editing, Writing – original draft, Supervision, Project administration, Conceptualization. **Ana María Sepúlveda:** Investigation. **Ana María Castañeda-Cifuentes:** Investigation. **Christine Frances:** Writing – review & editing, Writing – original draft, Supervision. **Johanna Pedroza-Díaz:** Writing – review & editing, Writing – original draft, Visualization, Supervision.

Funding

This research was funded by the Colombian Ministry of Science, Technology, and Innovation through the Doctorado en el Exterior program (Grant No. 885), managed by Colfuturo. The authors also acknowledge the National Polytechnic Institute of Toulouse (Toulouse INP) and the Chemical Engineering Laboratory (LGC) for supporting the researchers' stay in Colombia, which made this work possible.

Declaration of competing interest

The authors declare that they have no known competing financial interests or personal relationships that could have appeared to influence the work reported in this paper.

Acknowledgments

We would like to thank ITM Translation Agency (traducciones@itm.edu.co) for editing the manuscript in English.

Data availability

Data will be made available on request.

References

[1] P. Tavolaro, S. Catalano, A. Tavolaro, Anticancer activity modulation of an innovative solid formulation of extra virgin olive oil by cultured zeolite scaffolds, Food Chem. Toxicol. 124 (2019) 139–150, https://doi.org/10.1016/J.FCT.2018.11.061.

[2] WHO, IARC cancer today. https://www.who.int/en/news-room/fact-sheets/detail/cancer, 2025.

[3] W. Leowattana, P. Leowattana, T. Leowattana, Systemic treatment for metastatic colorectal cancer, World J. Gastroenterol. 29 (10) (2023) 1569–1588, https://doi.org/10.3748/wjg.v29.i10.1569.

[4] S. Blondy, V. David, M. Verdier, M. Mathonnet, A. Perraud, N. Christou, 5-Fluorouracil resistance mechanisms in colorectal cancer: from classical pathways to promising processes, Cancer Sci. 111 (9) (2020) 3142–3154, https://doi.org/10.1111/cas.14532.

[5] E.J. Kuipers, W.M. Grady, D. Lieberman, T. Seufferlein, J.J. Sung, P.G. Boelens, C.J. H. van de Velde, T. Watanabe, Colorectal cancer, Nat. Rev. Dis. Primers 176 (3) (2016) 139–148, https://doi.org/10.1038/nrdp.2015.65.

[6] R. Ahmad, J.K. Singh, A. Wunnava, O. Al-Obeed, M. Abdulla, S.K. Srivastava, Emerging trends in colorectal cancer: dysregulated signaling pathways (Review), Int. J. Mol. Med. 47 (3) (2021) 1–25, https://doi.org/10.3892/ijmm.2021.4847.

[7] A.M.L. Seca, D.C.G.A. Pinto, Plant secondary metabolites as anticancer agents: successes in clinical trials and therapeutic application, Int. J. Mol. Sci. 19 (1) (2018), https://doi.org/10.3390/ijms19010263.

[8] S. Hayakawa, T. Ohishi, N. Miyoshi, Y. Oishi, Y. Nakamura, M. Isemura, Anti-Cancer effects of green tea Epigallocatchin-3-Gallate and coffee chlorogenic acid, Molecules 25 (4553) (2020) 1–22, https://doi.org/10.3390/molecules25194553.

[9] H. Villota, G.A. Santa-González, D. Uribe, I.C. Henao, J.C. Arroyave-Ospina, C. J. Barrera-Causil, J. Pedroza-Díaz, Modulatory effect of chlorogenic acid and coffee extracts on Wnt/β-Catenin pathway in colorectal cancer cells, Nutrients 14 (22) (2022) 1–19, https://doi.org/10.3390/nu14224880.

[10] M.R. Olthof, P.C.H. Hollman, M.B. Katan, Chlorogenic acid and caffeic acid are absorbed in humans, J. Nutr. 131 (1) (2001) 66–71, https://doi.org/10.1093/JN/131.1.66.

[11] M.J. Rein, M. Renouf, C. Cruz-Hernandez, L. Actis-Goretta, S.K. Thakkar, M. da Silva Pinto, Bioavailability of bioactive food compounds: a challenging journey to bioefficacy, Br. J. Clin. Pharmacol. 75 (3) (2013) 588–602, https://doi.org/10.1111/J.1365-2125.2012.04425.X.

[12] R.J. Bułdak, T. Hejmo, M. Osowski, Ł. Bułdak, M. Kukla, R. Polaniak, E. Birkner, The impact of coffee and its selected bioactive compounds on the development and progression of colorectal cancer in vivo and in vitro, Molecules 23 (12) (2018) 1–26, https://doi.org/10.3390/molecules23123309.

[13] S. Rahaiee, E. Assadpour, A. Faridi Esfanjani, A.S. Silva, S.M. Jafari, Application of nano/microencapsulated phenolic compounds against cancer, Adv. Colloid Interface Sci. 279 (2020) 102153.

[14] M. Zare, Z. Norouzi Roshan, E. Assadpour, S.M. Jafari, Improving the cancer prevention/treatment role of carotenoids through various nano-delivery systems, Crit. Rev. Food Sci. Nutr. (2020) 1–13.

[15] B. Kim, J.E. Park, E. Im, Y. Cho, J. Lee, H.J. Lee, D.Y. Sim, W.Y. Park, B.S. Shim, S. H. Kim, Recent advances in nanotechnology with nano-phytochemicals: molecular mechanisms and clinical implications in cancer progression, Int. J. Mol. Sci. 22 (7) (2021), https://doi.org/10.3390/ijms22073571.

[16] Z. Zhang, X. Li, S. Sang, D.J. McClements, L. Chen, J. Long, A. Jiao, Z. Jin, C. Qiu, Polyphenols as plant-based nutraceuticals: health effects, encapsulation, Nano-Delivery, and application, Foods 11 (15) (2022) 1–17, https://doi.org/10.3390/foods11152189.

[17] M. Pourmadadi, S.E. Gerami, N. Ajalli, F. Yazdian, A. Rahdar, S. Fathi-karkan, M. A. Aboudzadeh, Novel pH-responsive hybrid hydrogels for controlled delivery of curcumin: overcoming conventional constraints and enhancing cytotoxicity in MCF-7 cells, Hybrid Adv. 6 (2024) 100210, https://doi.org/10.1016/J.HYBADV.2024.100210.

[18] M. Pourmadadi, A.R. Hafezi, S. Mafirad, M. Nouri, M. Shirazi, M. Younesi, N. Ajalli, A. Rahdar, S. Fathi-karkan, A.R. Del Bakhshayesh, A. Ghadami, L.F. Romanholo Ferreira, Development and evaluation of SA/PVP/γ-Al_2O_3 nanocarriers for targeted delivery of curcumin in colon cancer therapy, J. Drug Deliv. Sci. Technol. 105 (2025) 106632, https://doi.org/10.1016/J.JDDST.2025.106632.

[19] P.N. Ezhilarasi, P. Karthik, N. Chhanwal, C. Anandharamakrishnan, Nanoencapsulation techniques for food bioactive components: a review, Food Bioprocess Technol. 6 (3) (2013) 628–647, https://doi.org/10.1007/s11947-012-0944-0.

[20] C. Arpagaus, A. Collenberg, D. Rütti, E. Assadpour, S.M. Jafari, Nano spray drying for encapsulation of pharmaceuticals, Int. J. Pharm. 546 (1–2) (2018) 194–214, https://doi.org/10.1016/j.ijpharm.2018.05.037.

[21] S.K. Owusu-Ware, B.Z. Chowdhry, S.A. Leharne, M.D. Antonijević, Quantitative analysis of overlapping processes in the non-isothermal decomposition of chlorogenic acid by peak fitting, Thermochim. Acta 565 (2013) 27–33, https://doi.org/10.1016/j.tca.2013.04.029.

[22] I. Nallamuthu, A. Devi, F. Khanum, Chlorogenic acid loaded chitosan nanoparticles with sustained release property, retained antioxidant activity and enhanced bioavailability, Asian J. Pharm. Sci. 10 (3) (2015) 203–211, https://doi.org/10.1016/j.ajps.2014.09.005.

[23] A. Pettignano, A. Charlot, E. Fleury, Solvent-Free synthesis of amidated carboxymethyl cellulose derivatives : effect on the thermal properties, Polymers 11 (1227) (2019).

[24] B. Başyiğit, H. Sağlam, Ş. Kandemir, A. Karaaslan, M. Karaaslan, Microencapsulation of sour cherry oil by spray drying: evaluation of physical morphology, thermal properties, storage stability, and antimicrobial activity, Powder Technol. 364 (2020) 654–663, https://doi.org/10.1016/j.powtec.2020.02.035.

[25] T. Churam, P. Usubharatana, H. Phungrassami, Sustainable production of carboxymethyl cellulose: a biopolymer alternative from sugarcane (Saccharum officinarum L.) leaves, Sustainability 16 (6) (2024), https://doi.org/10.3390/su16062352.

[26] E. Boel, R. Koekoekx, S. Dedroog, I. Babkin, M.R. Vetrano, C. Clasen, G. Van den Mooter, Unraveling particle formation: from single droplet drying to spray drying and electrospraying, Pharmaceutics 12 (7) (2020) 1–58, https://doi.org/10.3390/pharmaceutics12070625.

[27] P.R. Sarika, N.R. James, P.R.A. Kumar, D.K. Raj, T.V. Kumary, Gum arabic-curcumin conjugate micelles with enhanced loading for curcumin delivery to hepatocarcinoma cells, Carbohydr. Polym. 134 (2015) 167–174, https://doi.org/10.1016/j.carbpol.2015.07.068.

[28] E.Y. So, M. Ouchi, S. Cuesta-Sancho, S.L. Olson, D. Reif, K. Shimomura, T. Ouchi, Tumor suppression by resistant maltodextrin, Fibersol-2, Cancer Biol. Ther. 16 (3) (2015) 460, https://doi.org/10.1080/15384047.2015.1009269.

[29] S.C. Sancho, S.L. Olson, E. Young So, K. Shimomura, T. Ouchi, F. Preuss, Fibersol-2 induces apoptosis of Apc-deficient colorectal Cancer (SW480) cells and decreases polyp formation in Apc MIN mice, Cancer Biol. Ther. 17 (6) (2016) 657–663, https://doi.org/10.1080/15384047.2016.1177685.

[30] S. AlYafii, Molecular mechanisims underlying the anticancer activity of gum arabic from acacia sp. in triple-negative breast cancer cells, in: United Arab Emirates University Scholarworks@Uaeu Theses, 2021. https://scholarworks.uaeu.ac.ae/all_theses/1089.

[31] A. Hassani, M.M.S. Azarian, W.N. Ibrahim, S.A. Hussain, Preparation, characterization and therapeutic properties of gum arabic-stabilized gallic acid nanoparticles, Sci. Rep. 10 (1) (2020) 1–18, https://doi.org/10.1038/S41598-020-71175-8.

[32] A.L.N. Avelino, N.V. R.e. Silva, G. B. De Oliveira, A.A.D.S. Silva, B.C. Cavalcanti, F. V.F. Jamacaru, C.A. Dornelas, Antioxidant and antigenotoxic actions of gum Arabic on the intestinal mucosa, liver and bone marrow of Swiss mice submitted to colorectal carcinogenesis, Nutr. Cancer 74 (3) (2022) 956–964, https://doi.org/10.1080/01635581.2021.1931699.

[33] D.M. Evans, J. Fang, T. Silvers, R. Delosh, J. Laudeman, C. Ogle, R. Reinhart, M. Selby, L. Bowles, J. Connelly, E. Harris, J. Krushkal, L. Rubinstein, J. H. Doroshow, B.A. Teicher, Exposure time versus cytotoxicity for anticancer agents, Cancer Chemother. Pharmacol. 84 (2) (2019) 359, https://doi.org/10.1007/S00280-019-03863-W.

[34] L. Niu, Z. Li, W. Fan, X. Zhong, M. Peng, Z. Liu, Nano-Strategies for enhancing the bioavailability of tea polyphenols: preparation, applications, and challenges, Foods 11 (3) (2022) 387, https://doi.org/10.3390/FOODS11030387, 387 2022 11.

[35] J.P. Cejas, A.S. Rosa, M.A. Nazareno, E.A. Disalvo, M.A. Frias, Interaction of chlorogenic acid with model lipid membranes and its influence on antiradical activity, Biochim. Biophys. Acta Biomembr. 1863 (1) (2021) 183484, https://doi.org/10.1016/J.BBAMEM.2020.183484.

[36] M. Boncler, J. Golanski, M. Lukasiak, M. Redzynia, J. Dastych, C. Watala, A new approach for the assessment of the toxicity of polyphenol-rich compounds with the use of high content screening analysis, PLoS One 12 (6) (2017), https://doi.org/10.1371/JOURNAL.PONE.0180022.

[37] O. Pechanova, E. Dayar, M. Cebova, Therapeutic potential of polyphenols-loaded polymeric nanoparticles in cardiovascular System, Molecules 25 (15) (2020) 3322, https://doi.org/10.3390/MOLECULES25153322.

[38] B. Wu, K. Kulkarni, S. Basu, S. Zhang, M. Hu, First-pass metabolism via UDP-glucuronosyltransferase: a barrier to oral bioavailability of phenolics, J. Pharmaceut. Sci. 100 (2011) 3655–3681, https://doi.org/10.1002/jps.22568.

[39] M. Liu, Q. Wang, F. Liu, X. Cheng, X. Wu, H. Wang, M. Wu, Y. Ma, G. Wang, H. Hao, UDP-Glucuronosyltransferase 1A compromises intracellular accumulation and anti-cancer effect of tanshinone IIA in human Colon cancer cells, PLoS One 8 (11) (2013), https://doi.org/10.1371/JOURNAL.PONE.0079172.

[40] K.W. Kang, M.K. Chun, O. Kim, R.K. Subedi, S.G. Ahn, J.H. Yoon, H.K. Choi, Doxorubicin-loaded solid lipid nanoparticles to overcome multidrug resistance in cancer therapy, Nanomed. Nanotechnol. Biol. Med. 6 (2) (2010) 210–213, https://doi.org/10.1016/J.NANO.2009.12.006.

[41] Y.J. Wang, Y. Huang, N. Anreddy, G.N. Zhang, Y.K. Zhang, M. Xie, D. Lin, D. H. Yang, M. Zhang, Z.S. Chen, Tea nanoparticle, a safe and biocompatible nanocarrier, greatly potentiates the anticancer activity of doxorubicin, Oncotarget 7 (5) (2016) 5877–5891, https://doi.org/10.18632/ONCOTARGET.6711.

[42] S. Li, C. Li, S. Jin, J. Liu, X. Xue, A.S. Eltahan, J. Sun, J. Tan, J. Dong, X.J. Liang, Overcoming resistance to cisplatin by inhibition of glutathione S-transferases (GSTs) with ethacraplatin micelles in vitro and in vivo, Biomaterials 144 (2017) 119–129, https://doi.org/10.1016/j.biomaterials.2017.08.021.

[43] N. Hou, N. Liu, J. Han, Y. Yan, J. Li, Chlorogenic acid induces reactive oxygen species generation and inhibits the viability of human colon cancer cells, Anti Cancer Drugs 28 (1) (2017) 59–65, https://doi.org/10.1097/CAD.0000000000000430.

[44] A.A. Neamțu, T.A. Maghiar, V. Turcuș, P.B. Maghiar, A.M. Căpraru, B.A. Lazar, C. A. Dehelean, O.L. Pop, C. Neamțu, B.D. Totolici, E. Mathe, A comprehensive view

on the impact of chlorogenic acids on colorectal cancer, Curr. Issues Mol. Biol. 46 (7) (2024) 6783–6804, https://doi.org/10.3390/CIMB46070405.
[45] S. Elmore, Apoptosis: a review of programmed cell death, Toxicol. Pathol. 35 (4) (2007) 495–516, https://doi.org/10.1080/01926230701320337.
[46] J. Xu, A.M. Elshazly, D.A. Gewirtz, The cytoprotective, cytotoxic and nonprotective functional forms of autophagy induced by microtubule poisons in tumor Cells—Implications for autophagy modulation as a therapeutic strategy, Biomedicines 10 (7) (2022) 1632, https://doi.org/10.3390/BIOMEDICINES10071632.
[47] V.V. Veselov, A.E. Nosyrev, L. Jicsinszky, R.N. Alyautdin, G. Cravotto, Targeted delivery methods for anticancer drugs, Cancers 14 (3) (2022) 622, https://doi.org/10.3390/cancers14030622.
[48] S. Razzaq, I. Fatima, Z. Moafian, A. Rahdar, S. Fathi-karkan, Z. Kharaba, M. Shirzad, A. Khan, S. Pandey, Nanomedicine innovations in colon and rectal cancer: advances in targeted drug and gene delivery systems, Med. Oncol. 42 (4) (2025) 1–35, https://doi.org/10.1007/S12032-025-02670-Z/METRICS.